Journal of Materials Chemistry C

Accepted Manuscript

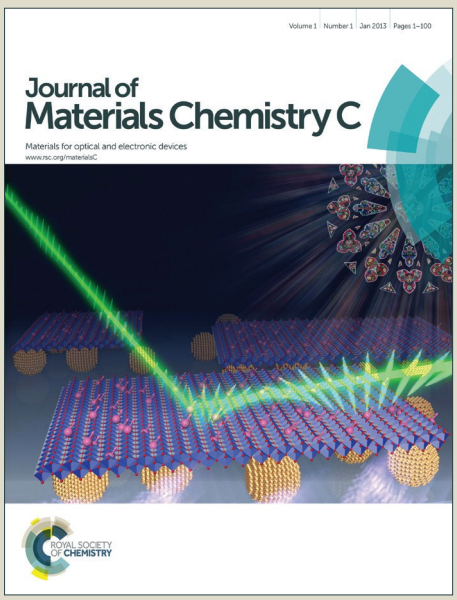

ROYAL SOCIETY OF CHEMISTRY

www.rsc.org/materialsC

Journal Name

COMMUNICATION

Co-doped Sb_2Te_3 Paramagnetic Nanoplates

Lei Yang,[a] Zhi-Gang Chen,[a*] Tianxiao Nie,[b] Guang Han,[a] Zhi Zhang,[a] Min Hong,[a] Kang L Wang,[b] and Jin Zou [a,c*]

Received 00th January 20xx,
Accepted 00th January 20xx

DOI: 10.1039/x0xx00000x

www.rsc.org/

Co-doped Sb_2Te_3 nanoplates are fabricated by a facile and green solvothermal method. The as-synthesized nanoplates show uniform hexagonal morphology with a distribution of 1-2 μm in diameters and ~ 50 nm in thickness. The detailed structural and compositional characterizations indicates that Co uniformly distributes in Sb_2Te_3 and leads to a lattice shrink of 1.22% along the *a* axis and 0.9% along the *c* axis. A Superconducting Quantum Interference Device magnetometer is used to determine the temperature dependent magnetization in zero-field cooled and field cooled processes. It is found the paramagnetic state in our Co-doped Sb_2Te_3 nanoplates from 5 K to 300 K.

Introduction

Antimony telluride (Sb_2Te_3) has been extensively studied due to its multi-discipline application as topological insulators,[1, 2] and thermoelectric materials.[3, 4] On the basis of theoretical calculations,[1, 2] Sb_2Te_3 has robust and simple conducting surface states with a single gapless Dirac cone at the Γ point. Additionally, several unique physical phenomena, namely, quantum hall effect,[1, 2] quantized anomalous Hall effect,[5] and topological magnetoelectric effect,[6-8] have been theoretically predicted and experimentally demonstrated in Sb_2Te_3. Especially, introducing magnetic impurities, such as Fe,[9] into Sb_2Te_3 can break the time reversal symmetry, inducing a gap at the Dirac point of the topological surface state,[10] which is crucial for realizing exotic phenomena mentioned above.[1, 5, 10, 11] Therefore, the further understanding of the coexistence of both topological state and magnetic order in topological materials should be highly prompted.

According to the theoretical calculations and experimental results,[3, 4, 7, 12, 13] the electrical and magnetic properties of Sb_2Te_3 can be tuned by the substitution of transition metals, such as Fe,[9] Cr,[8, 14] Mn,[15, 16] and V,[17, 18] to obtain dilute magnetic semiconductors from the diamagnetic un-doped Sb_2Te_3.[19, 20] For example, Zhang *et al.*[13] suggested that cation-site substitution in the anion-rich environment is the most effective doping method. Under the nominal dopant concentration of 4%, Cr-doped Sb_2Te_3 remain as insulators, while the V- , Mn- and Fe-doped Sb_2Te_3 become metallic.[13] In another study, ferromagnetic ordering was observed in Mn-doped Sb_2Te_3 compounds at a Curie temperature (T_C) of 17 K.[21] Furthermore, the T_C of Sb_2Te_3 can be tuned by adjusting the doping level in the dilute magnetic semiconductor p-type $Sb_{2-x}Cr_xTe_3$,[8] in which ferromagnetism was observed at T_C ~ 5.8 K for x = 0.0215 and at T_C ~ 2.0 K for x = 0.0115, respectively. However, most of these studies were performed in bulk materials; and magnetic properties of doped Sb_2Te_3 nanostructures have rarely been investigated. Recently, nanostructured topological insulators have drawn much attention due to their novel physical properties,[22-24] which is exciting for the future development of new-generation spintronic devices. Due to the size effect, it is easier to manipulate the surface state of nanostructures when compared to their bulk counterparts,[22-25] which makes them as preferred candidates for the practical applications in spintronic nano-devices.

In this study, we employed a facile and controllable solvothermal approach[25, 26] to realize Co doping into hexagonal shaped Sb_2Te_3 nanoplates. From our detailed structural and chemical characterizations, we found that Co ions are uniformly doped into Sb_2Te_3, resulting in a slight lattice shrink from the equilibrium Sb_2Te_3 crystal structure and introducing atomic moment in the Sb_2Te_3 lattice. The obtained Co-doped Sb_2Te_3 nanoplates reveal a paramagnetic behavior from 5 to 300 K.

Experimental

The Co-doped Sb_2Te_3 nanoplates were solvothermally synthesized, in which analytical grade Sb_2O_3, Te, $CoCl_2$, ethylene glycol, polyvinylpyrrolidone (PVP) and NaOH solution were used as the precursors. In a typical synthesis, 0.2 g of PVP was first dissolved in ethylene glycol (36 mL) to form a clear solution, followed by adding Sb_2O_3, $CoCl_2$, and Te powders with defined ratios to achieve $Sb_{1.9}Co_{0.1}Te_3$. After stirring for 5 min, the prepared solution was mixed with 4 mL of NaOH solution (5 mol/L), the resulting suspension was stirred vigorously for 30 min at 65 °C, and subsequently sealed in a 120 ml autoclave. The autoclave was then heated to 230 °C in an oven and maintained at this temperature for 24 h, then cooled naturally to the room temperature. The synthesized products were collected by a high-speed centrifugation,

[a] *Materials Engineering, The University of Queensland, Brisbane, QLD 4072, Australia.*
[b] *University of California in Los Angeles, Department of Electrical Engineering, Device Research Laboratory, Los Angeles, CA 90095 USA.*
[c] *Centre for Microscopy and Microanalysis, The University of Queensland, Brisbane, QLD 4072, Australia.*
* E-mail: j.zou@uq.edu.au, z.chen1@uq.edu.au

washed 6 times with distilled water and absolute ethanol, and finally dried at 50 °C for 12 h.

The structural feature of synthesized products were investigated by X-ray diffraction (XRD), recorded on an X-ray diffractometer equipped with graphite monochromatized, in which the Cu Kα radiation (λ = 1.5418 Å) was employed. The morphological, structural, and chemical characteristics of as-synthesized products were investigated using scanning electron microscopy (SEM, JEOL 7800F, operated at 5 kV) and transmission electron microscopy (TEM, Philips FEI Tecnai F20, operated at 200 kV, equipped with an electron Energy-dispersive X-ray spectroscopy (EDS) and an electron energy loss spectroscopy (EELS) system for chemical analysis). A Superconducting Quantum Interference Device (SQUID) magnetometer was used to obtain the temperature dependent magnetization in zero-field cooled (ZFC) and field cooled (FC) processes.

Results and Discussion

Fig. 1(a) shows the XRD pattern of as-synthesized Co-doped Sb_2Te_3 (blue pattern) and un-doped Sb_2Te_3 (black pattern) products compared with the diffraction peaks (red) of the rhombohedral structured Sb_2Te_3 found in the standard identification card (JCPDS 15-0874, lattice parameters $a = b = 4.262$ Å and $c = 30.48$ Å), in which all diffraction peaks can be exclusively indexed as the Sb_2Te_3 phase with the space group of $R\bar{3}m$. There is no secondary phase or any observable impurities, indicating the high purity of our synthesized products. Nevertheless, our detailed comparison of obtained XRD pattern of Co-doped and un-doped Sb_2Te_3 diffraction peaks shows that the diffraction peaks of as-synthesized Co-doped Sb_2Te_3 products have right-shifted, indicating the existence of a lattice shrink in as-synthesized products. Fig. 1(b) shows the enlarged 0006* and $11\bar{2}0$* diffraction peaks of Co-doped Sb_2Te_3 compared with diffraction peaks of un-doped Sb_2Te_3, from which the lattice parameters of as-synthesized Co-doped Sb_2Te_3 products can be determined as a = 4.20 Å and c = 30.20 Å - revealing a decrease of 1.22% along the a axis and a decrease of 0.9% along the c axis, respectively. This lattice shrinkage could be caused by the substitution of Sb ions by the relatively smaller Co ions. Fig. 1(c) shows a representative SEM image of the as-synthesized products, in which plate-shaped nanostructures can be observed with a lateral dimension of 1-2 μm. Fig. 1(d) is a zoom-in SEM image showing a typical hexagonal-shaped Co-doped Sb_2Te_3 nanoplate, and the inset shows a ~ 50nm thick nanoplate.

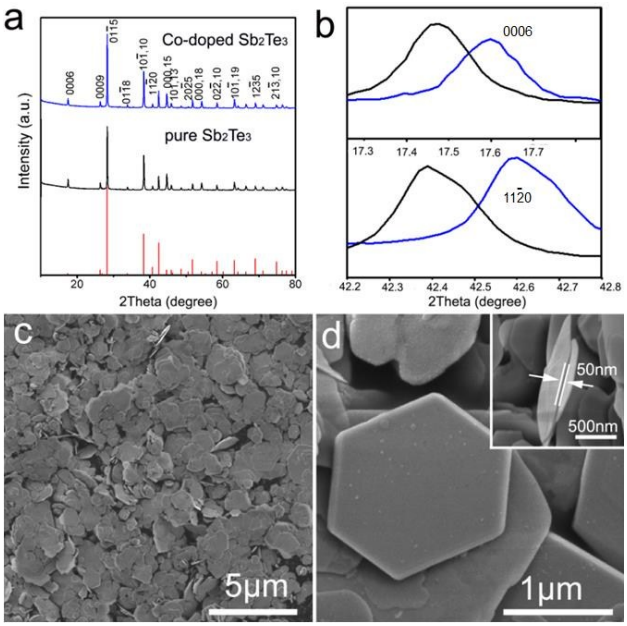

Figure 1 (a) XRD patterns of Co-doped Sb_2Te_3 and un-doped Sb_2Te_3 compared with diffraction peaks of the rhombohedral structured Sb_2Te_3 phase; (b) Enlarged 0006* and $11\bar{2}0$* peaks of Co-doped Sb_2Te_3 (blue) compared with un-doped Sb_2Te_3 peaks (black); (c) SEM image showing high-yield of the synthesis; (d) High magnification SEM image showing a typical hexagonal-shaped nanoplate, and the inset showing the thickness of a typical nanoplate.

To understand the structural characteristics of as-synthesized Co-doped Sb_2Te_3 nanoplates, detailed TEM investigations were employed. Fig. 2(a) is a TEM image showing a typical hexagonal-shaped nanoplate, its lateral dimension fits well with the lateral dimension determined by SEM. Fig. 2(b)-(c) show corresponding selected area electron diffraction (SAED) patterns and high resolution TEM (HRTEM) image, both showing the surface normal of the nanoplate is parallel to its c axis. By close correlating the six side edges shown Fig. 2(a) and the indexed diffraction spots in Fig. 2(b), the side edges of the nanoplates can be determined to be {$10\bar{1}0$} facets. It is of interest to note that the transparent feature of this nanoplate shown in Fig. 2(a) and easy of taking HRTEM image

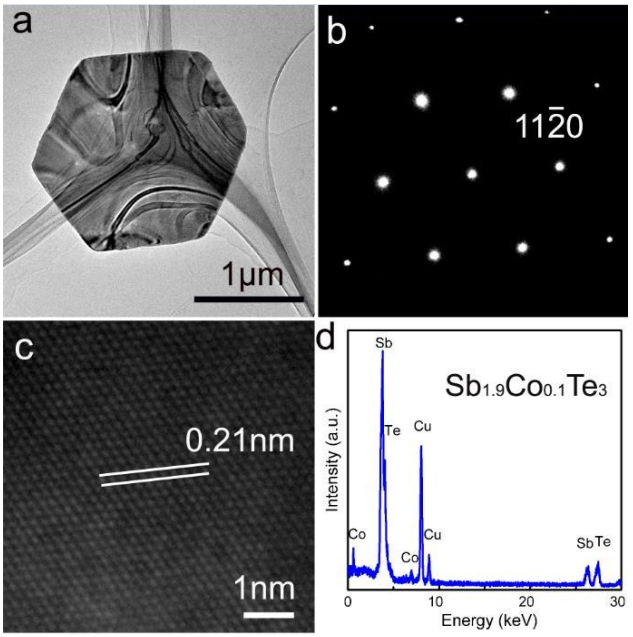

Figure 2 (a) TEM image for a thin nanoplate; (b) Corresponding SAED pattern; (c) Corresponding HRTEM image; (d) Corresponding EDS spectrum.

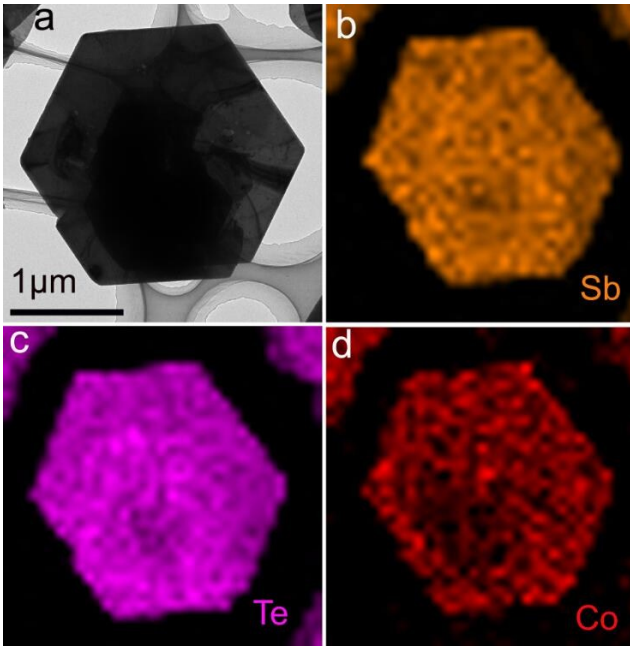

Figure 3 (a) A typical TEM image of Co-doped Sb_2Te_3 nanoplate; (b)-(d) EDS maps for Sb, Te and Co, respectively.

shown in Fig. 2(c) suggest that this nanoplate is very thin (< 30 nm). In addition, the facts of the sharp diffraction spots shown in Fig. 2(b) and the nature of perfect crystalline found in Fig. 2(c) indicate that our synthesized nanoplates are well-crystalized with no observable lattice defects. To elucidate compositional characteristics of as-synthesized Co-doped Sb_2Te_3 nanoplates, EDS was used to determine their chemical compositions and distributions. Fig. 2(d) is the corresponding EDS spectrum for a typical Co-doped Sb_2Te_3 nanoplate, from which, Co, Te and Sb peaks can be clearly observed while Cu peaks are due to the Cu TEM grid. According to our quantitative EDS analysis, the composition of our Co-doped Sb_2Te_3 nanoplates can be determined as $Sb_{1.9}Co_{0.1}Te_3$.

To clarify how Co is incorporated in the binary Sb_2Te_3, EDS mappings were performed. Fig. 3(a) is a TEM image of a nanoplate, and Fig. 3(b)-(d) are EDS maps for Sb, Te and Co, respectively. The relative uniform contrast of the Co map [refer Fig. 3(d), in which the dotted contrast is caused by the rough probe size] suggested that Co has uniformly distributed in the nanoplate.

To investigate the valence state of Co, EELS analysis was applied. Fig. 4(a) shows an EELS profile acquired from an as-prepared Co-doped Sb_2Te_3 nanoplate, in which Te-$M_{4,5}$ edges and Co-$L_{2,3}$ edges can be clearly observed in an energy loss region between 600 and 1000 eV. Especially, the existence of Co-$L_{2,3}$ edges provides the direct evidence of the substitution of Sb ions by Co ions,[25, 26] the corresponding atomic

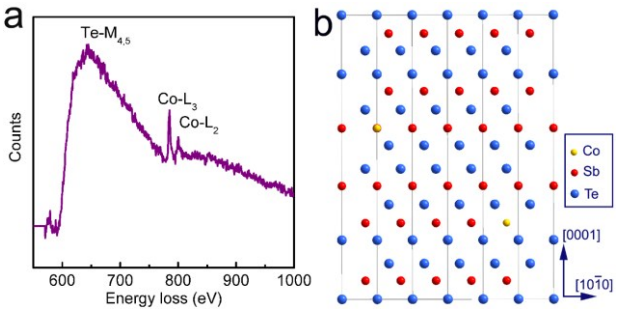

Figure 4 (a) EELS spectrum of a Co-doped Sb_2Te_3 nanoplate showing the Te-$M_{4,5}$ and Co-$L_{2,3}$ edges; (b) Atomic model illustrating the substitution of Sb ions by Co ions in the Co-doped Sb_2Te_3 nanoplate.

model can be schematically illustrated in Fig. 4(b).

Above detailed structural characterizations confirmed that Co has been successfully doped into Sb_2Te_3 by substituting Sb ions. On this basis, new magnetic properties may be introduced in our Co-doped Sb_2Te_3 nanoplates, which needs verifying. A SQUID magnetometer was used to obtain the temperature dependent magnetization in zero-field cooled (ZFC) and field cooled (FC) processes. The sample was cooled in the absence of a magnetic field from 300 K down to 5 K and then the magnetization was measured from 5 to 300 K under a magnetic field of 100 Oe, the temperature-dependent ZFC and FC plots are showed in Fig. 5(a). As can be seen, the ZFC and FC curves are almost identical, no obvious turning point can be found within the measuring temperature range of 5-300 K, indicating that the Co-doped Sb_2Te_3 nanoplates show similar magnetic state in this temperature range no matter whether the magnetic field was applied or not. The magnetic field dependent magnetization and hysteresis (*M-H*) loops were obtained at 5 K and 20 K, respectively, and the results are showed in Fig. 5(b). The *M-H* curve reveals the typical paramagnetic behaviour of Co-doped Sb_2Te_3 nanoplates at both *T*= 5 K and 20 K, which is significantly different with diamagnetic un-doped Sb_2Te_3[19, 20] and ferromagnetism Cr-, Fe- and Mn-doped Sb_2Te_3[8, 9, 15] and the doping of Co ions was considered originating the magnetic moments because the pure Sb_2Te_3 is diamagnetic. Curie constant (*C*) can be determined to further understand the contribution of Co ions to the paramagnetism.[26] Fig.

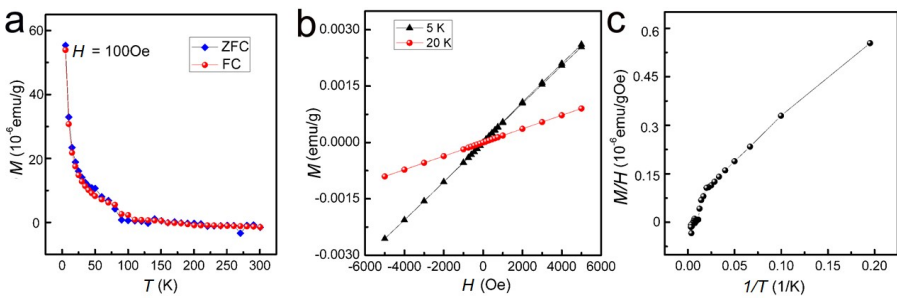

Figure 5 (a) Temperature dependent magnetization moments in ZFC and FC processes under the field of 100 Oe; (b) *M-H* profiles at temperatures of 5 K and 20 K; (c) *H/M* plot of ZFC curve under the field of 100 Oe as a function of (1/*T*), the slope corresponding to the Curie constant.

5(c) is the re-plotted figure from Fig. 5(a), where the *C* value can be determined by obtaining the slop of the plot shown in Fig. 5(c) as *C* = 3.18 ×10^{-6} emu K/g Oe according to the Curie law *C*= *MT/H,*[27] where *M* is the resultant magnetization, *H* is the magnetic field, and *T* is absolute temperature. Moreover, the susceptibility (χ) of the paramagnetic materials in a small field can be expressed as[27] $\chi = N\mu_0\mu^2/3k_BT = M/H$ with the Langevin paramagnetic function, where *N* is the number of magnetic atoms per unit gram (in our Co-doped Sb_2Te_3, the number of Co can be estimated as 6.452×10^{19} per unit gram due to the chemical composition has been estimated as $Sb_{1.9}Co_{0.1}Te_3$), μ is the effective moment of a magnetic atom, μ_0 is vacuum permeability which is 1 in the centimetre–gram– second unit system and is dimensionless, and k_B is Boltzmann constant (1.38×10^{-23} J/K). In our study, μ= 1.42 ×10^{-24}J/T can be calculated by combining Curie law with the Langevin paramagnetic function. We can definite that each doped Co ion in our $Sb_{1.9}Co_{0.1}Te_3$ system distributes an effective moment of $\mu=x\mu_B$ when we consider the doping of Co ions originating the magnetic moments, where *x* is the amount of Bohr magneton from each doped Co ion and μ_B is the Bohr magneton[27] (9.274×10^{-24} J/T). Therefore, *x* can be determined as 0.15, which means every Co ion has an effective moment of 0.15μ_B in our $Sb_{1.9}Co_{0.1}Te_3$ nanoplates. The magnetic moments originated from doped Co ions and the paramagnetic behaviour are contributed from the spin polarization of electric band structure. These findings of paramagnetic $Sb_{1.9}Co_{0.1}Te_3$ nanoplates provide a significant progress in developing nanoelectronic and spintronic devices.

Conclusions

In this study, the compositional uniform and hexagonal-shaped $Sb_{1.9}Co_{0.1}Te_3$ nanoplates were synthesized by a facile solvothermal method. Based on our detailed morphological, structural, chemical characteristics, we found that Co ions have substituted Sb ions in the crystal lattice, leading to (1) reduced lattice parameters, and (2) paramagnetic state from 5K to the room temperature. This study paves a way to develop magnetic Sb_2Te_3 topological insulators for design and development of future electronic and spintronic devices.

Acknowledgements

This work was financially supported by the Australian Research Council, ZGC thanks QLD government for a smart state future fellowship (2011002414). LY thanks the China Scholarship Council for providing his PhD stipend. The Australian Microscopy & Microanalysis Research Facility is acknowledged for providing characterization facilities.

Notes and references

1. H. Zhang, C.-X. Liu, X.-L. Qi, X. Dai, Z. Fang and S.-C. Zhang, *Nat. Phys.*, 2009, **5**, 438.
2. L. Zhao, H. Deng, I. Korzhovska, Z. Chen, M. Konczykowski, A. Hruban, V. Oganesyan and L. Krusin-Elbaum, *Nat. Mater.*, 2014, **13**, 580.
3. V. A. Kulbachinskii, V. G. Kytin, A. A. Kudryashov and P. M. Tarasov, *J. Solid State Chem.*, 2012, **193**, 47.
4. V. A. Kulbachinskii, V. G. Kytin, A. A. Kudryashov and P. M. Tarasov, in *Magnetism and Magnetic Materials V*, eds. N. Perov and V. Rodionova, 2012, vol. 190, pp. 558.
5. R. Yu, W. Zhang, H.-J. Zhang, S.-C. Zhang, X. Dai and Z. Fang, *Science*, 2010, **329**, 61.
6. V. A. Kulbachinskii, P. V. Gurin, P. M. Tarasov, A. B. Davydov, Y. A. Danilov and O. V. Vikhrova, *Low. Temp. Phys.*, 2007, **33**, 174.
7. C. Drasar, J. Kasparova, P. Lostak, X. Shi and C. Uher, *Phys. Status Solidi B*, 2007, **244**, 2202.
8. V. A. Kulbachinskii, P. M. Tarasov and E. Bruck, *J. Exp. Theor. Phys.*, 2005, **101**, 528.
9. Z. H. Zhou, M. Zabeik, P. Lostak and C. Uher, *J. Appl. Phys.*, 2006, **99**, 043901.
10. G. Rosenberg and M. Franz, *Phys. Rev. B*, 2012, **85**, 195119.
11. V. A. Kulbachinskii, V. G. Kytin, A. A. Kudryashov and P. M. Tarasov, *9th European Conference on Thermoelectrics (Ect2011)*, 2012, **1449**, 95.
12. P. Larson and W. R. L. Lambrecht, *Phys. Rev. B*, 2008, **78**, 195207.
13. J.-M. Zhang, W. Ming, Z. Huang, G.-B. Liu, X. Kou, Y. Fan, K. L. Wang and Y. Yao, *Phys. Rev. B*, 2013, **88**, 235131.
14. Z. Zhou, Y.-J. Chien and C. Uher, *Phys. Rev. B*, 2006, **74**, 224418.
15. H. Luo, Q. Gibson, J. Krizan and R. J. Cava, *J. Phys-condens Mat.*, 2014, **26**, 206002.
16. J. Choi, H. W. Lee, B. S. Kim, S. Choi, J. Choi, J. H. Song and S. L. Cho, *J. Appl. Phys.*, 2005, **97**, 10D324.
17. J. S. Dyck, K. Ahilan, M. C. Aronson, C. Uher and P. Lost'ak, *Phys. Status Solidi B*, 2006, **243**, 1862.
18. J. S. Dyck, P. Hajek, P. Losit'ak and C. Uher, *Phys. Rev. B*, 2002, **65**, 115212.
19. Z. Zhou, M. Žabèík, P. Lošták and C. Uher, *J. Appl. Phys.*, 2006, **99**, 043901.
20. J. Horák, M. Matyáš and L. Tichý, *phys.a status solidi (a)*, 1975, **27**, 621.
21. J. Choi, S. Choi, J. Choi, Y. Park, H. M. Park, H. W. Lee, B. C. Woo and S. Cho, *Phys. Status Solidi B*, 2004, **241**, 1541.
22. H. Peng, W. Dang, J. Cao, Y. Chen, D. Wu, W. Zheng, H. Li, Z.-X. Shen and Z. Liu, *Nat. Chem.*, 2012, **4**, 281.
23. H. Peng, K. Lai, D. Kong, S. Meister, Y. Chen, X.-L. Qi, S.-C. Zhang, Z.-X. Shen and Y. Cui, *Nat. Mater.*, 2010, **9**, 225.
24. F. Xiu, L. He, Y. Wang, L. Cheng, L.-T. Chang, M. Lang, G. Huang, X. Kou, Y. Zhou, X. Jiang, Z. Chen, J. Zou, A. Shailos and K. L. Wang, *Nat. Nano.*, 2011, **6**, 216.
25. L. Cheng, Z. G. Chen, S. Ma, Z. D. Zhang, Y. Wang, H. Y. Xu, L. Yang, G. Han, K. Jack, G. Q. Lu and J. Zou, *J. Am. Chem. Soc.*, 2012, **134**, 18920.
26. Z.-G. Chen, L. Yang, S. Ma, L. Cheng, G. Han, Z.-d. Zhang and J. Zou, *Appl. Phys. Lett.*, 2014, **104**, 053105.
27. S. J. Blundell, *Magnetism in Condensed Matter*, Oxford University Press, 2001.

TOC